Measuring Unfolding of Proteins in the Presence of Denaturant Using Fluorescence Correlation Spectroscopy

Krishnananda Chattopadhyay, Saveez Saffarian, Elliot L. Elson, and Carl Frieden
Department of Biochemistry and Molecular Biophysics, Washington University School of Medicine, St. Louis, Missouri 63110

ABSTRACT IFABP is a small (15 kDa) protein consisting mostly of antiparallel β-strands that surround a large cavity into which ligands bind. We have previously used FCS to show that the native protein, labeled with fluorescein, exhibits dynamic fluctuation with a relaxation time of 35 μs. Here we report the use of FCS to study the unfolding of the protein induced by guanidine hydrochloride. Although the application of this technique to measure diffusion coefficients and molecular dynamics is straightforward, the FCS results need to be corrected for both viscosity and refractive index changes as the guanidine hydrochloride concentration increases. We present here a detailed study of the effects of viscosity and refractive index of guanidine hydrochloride solutions to calibrate FCS data. After correction, the increase in the diffusion time of IFABP corresponds well with the unfolding transition monitored by far ultraviolet circular dichroism. We also show that the magnitude of the 35 μs phase, reflecting the conformational fluctuation in the native state, decreases sharply as the concentration of denaturant increases and the protein unfolds. Although FCS experiments indicate that the unfolded state at pH 2 is rather compact and native-like, the radius in the presence of guanidine hydrochloride falls well within the range expected for a random coil.

INTRODUCTION

FCS is emerging as an important technique in biochemical studies to study diffusion as well as conformational transitions on timescales of microseconds and longer (Elson, 1985; Frieden et al., 2002; Hess et al., 2001). It involves measuring fluorescence fluctuations under conditions of thermodynamic equilibrium in a small observation volume. These fluctuations may result either from a change in the number of fluorophores in the observation volume due to diffusion or a change in fluorescence properties of the molecule as a consequence of a chemical reaction or a conformational fluctuation.

We have recently reported the application of FCS to study microsecond conformational dynamics of native IFABP (Chattopadhyay et al., 2002a). IFABP belongs to a family of proteins that bind a variety of ligands (fatty acids, bile salts, and retinoids) into a large cavity located in the interior of the protein. It is a small (15 kDa) monomeric protein consisting of two β-sheets, each containing five β-strands, and a small helical region (Fig. 1) (Hodsdon et al., 1996; Sacchettini et al., 1989). In an earlier study (Chattopadhyay et al., 2002a), we mutated Val-60, located in a turn between the D and E strands, to cysteine and covalently modified the protein with fluorescein. FCS studies showed that for this mutant (V60Flu), the data were best described using a model that includes both diffusion and an isomerization component. The isomerization rate was on the order of 35 μs and reflected a dynamic fluctuation of the fluorescein with respect to a neighboring Trp (Trp-82) that quenches the fluorescein fluorescence. The diffusion coefficient determined as a function of pH suggested the formation of a compact intermediate state at low pH before the unfolding transition of the protein.

In this study, we have extended the FCS measurements to the unfolding of the protein to determine the diffusion time and characteristics of the conformational change observed in the native protein as a function of denaturant concentration. In doing so, however, we found that FCS measurements in the presence of Gdn (or urea) are complicated due to changes in viscosity and refractive index. We have performed a systematic study to compensate for the effect of the aberrations induced by a refractive index mismatch in the presence of Gdn. Our results indicate that the change in diffusion time studied by FCS after minimizing the refractive index aberration follows the equilibrium unfolding transition monitored by far ultraviolet (UV) circular dichroism. The hydrodynamic radii of the protein in different folding states have been measured by FCS experiments, and the data match independent light-scattering measurements. Although the radius of the unfolded state of IFABP at pH 2 is compact, that in the presence of Gdn is identical to a random coil. Moreover, the magnitude of the microsecond conformational

Submitted September 17, 2004, and accepted for publication November 5, 2004.

Address reprint requests to Carl Frieden, Dept. of Biochemistry and Molecular Biophysics, Box 8231, Washington University School of Medicine, 660 S. Euclid Ave. St. Louis, MO 63110. Tel.: 314-362-3344; Fax: 314-362-7183; E-mail: frieden@biochem.wustl.edu.

Saveez Saffarian's present address is Dept. of Cell Biology, Harvard Medical School/CBR Institute for Biomedical Research, 200 Longwood Ave., Boston, MA 02115.

Abbreviations used: IFABP, rat intestinal fatty acid binding protein; FCS, fluorescence correlation spectroscopy; Gdn, guanidine hydrochloride; fluorescein, 5-iodo acetamido fluorescein; Alexa488, Alexa488 maleimide; V60Flu, fluorescein covalently linked to Cys-60 of the V60C mutant of IFABP; V60Alexa, Alexa488 covalently linked to Cys-60 of the V60C mutant of IFABP; F62Flu, fluorescein covalently linked to Cys-62 of the F62C mutant of IFABP; F62Alexa, Alexa488 covalently linked to Cys-62 of the F62C mutant of IFABP; and τ_R, chemical relaxation time.

0006-3495/05/02/1413/10 $2.00

doi: 10.1529/biophysj.104.053199

FIGURE 1 X-ray crystal structure of the intestinal fatty acid binding protein (Sacchettini et al., 1989). Positions and numbering of V60 and F62 are shown and labeled.

fluctuation observed in the native state decreases sharply as the protein unfolds.

MATERIALS AND METHODS

Mutagenic primers were obtained from Integrated DNA Technologies (Coralville, ID). The QuickChange site-directed mutagenesis kit was obtained from Stratagene (La Jolla, CA). Fluorescein and Alexa488 maleimide were purchased from Molecular Probes (Eugene, OR). Gdn was obtained from ICN Biochemicals (Aurora, OH). All other reagents used were analytical grade.

Expression and purification of the V60C and F62C mutants of IFABP were as described elsewhere (Jiang and Frieden, 1993). The reaction with fluorescein or with Alexa488 maleimide was carried out using a previously published procedure (Chattopadhyay et al., 2002a). For experiments as a function of Gdn, a series of protein solutions at different denaturant concentrations were prepared in 20 mM phosphate buffer at pH 7.3. The solutions were equilibrated at room temperature for 1 h before the measurements were performed.

Steady-state fluorescence experiments were performed at 20°C using a PTI Alphascan fluorometer (Photon Technology International, South Brunswick, NJ) and protein concentrations of ~1 μM. For fluorescein and Alexa488 modified proteins, the excitation wavelength was 488 nm and emission spectra were recorded between 500 nm and 600 nm. Circular dichroism experiments were performed on a Jasco J-715 using a 0.1 cm pathlength cell. For the unfolding experiments, the ellipticity at 216 nm was plotted against the concentration of the unfolding agents, and the unfolding transition was fit to a simple two-state model (Santoro and Bolen, 1988, 1992).

The light-scattering measurements were performed at 20°C using the DynaPro-801 light-scattering instrument (Protein Solutions, Charlottesville, VA). Two hundred μl of 2 mg/ml of V60C at different solution conditions (at pH 2 and pH 7 buffers, and also in presence of Gdn) were injected and the scattered light was detected using an avalanche photo diode. The data were collected and analyzed using DYNAMICS software provided with the instrument.

The procedure for FCS experiments using two-photon excitation has been described elsewhere (Chattopadhyay et al., 2002a) and the same experimental procedure has been used here. A laser beam from a titanium sapphire laser (Mira 900 radiation, Coherent, Palo Alto, CA) was directed to the side of an Olympus IX 70 microscope. A 5× beam expander was used to overfill the back aperture of an Olympus 60× water immersion objective. A dichroic mirror (725DCSPXR, Chroma Technology, Rockingham, VT) was used to reflect the laser beam toward the objective. The fluorescence from the samples was collected from the image plane on the side port of the microscope. The fluorescence, collimated by using a simple convex lens, was then passed through a 50/50 beam splitter and detected by using two avalanche photo diode units (photon counting module SPCM-QC, PerkinElmer Optoelectronics, Fremont, CA). The correlation function was calculated real time using a correlator card (http://correlator.com, ELEX01-08D). The beam profile was determined using a rhodamine sample in ethanol. All the data analyses were performed using Origin 7.0 (OriginLab, Northampton, MA).

For a single species with a diffusion time, τ_D, a correlation function of the form of Eq. 1 can be obtained:

$$G(\tau) = \frac{1}{N(1+\tau/\tau_D)} \frac{1}{\sqrt{1+\tau/S^2\tau_D}} + 1, \qquad (1)$$

where N is the number of particles in the observation volume and S is the depth/diameter ratio of the three-dimensional Gaussian volume element. FCS experiments using the free dye, Alexa488 maleimide, can be fit to Eq. 1. On the other hand, FCS experiments using fluorescently labeled Val-60 mutants of IFABP could not be analyzed satisfactorily using Eq. 1 as a result of a conformational fluctuation present in the native protein (Chattopadhyay et al., 2002a). If the diffusing species (with the diffusion time of τ_D) undergoes a chemical reaction or conformational change with a time constant of τ_R, the correlation function of the system can be represented by Eq. 2 (Haupts et al., 1998):

$$G(\tau) = \frac{1-A+A\exp(-\tau/\tau_R)}{N(1-A)} \frac{1}{1+\tau/\tau_D} \frac{1}{\sqrt{1+\tau/S^2\tau_D}} + 1, \qquad (2)$$

where A is the magnitude (or extent) of the τ_R process.

The radius, W, of the focal volume of the system can be calculated using Eq. 3,

$$\tau_D = \frac{W^2}{4D}, \qquad (3)$$

where D is the diffusion coefficient. For this purpose, FCS experiments were performed with rhodamine 6G for which D is known and consequently W can be calculated from the measured τ_D value.

RESULTS

Equilibrium unfolding transitions of wild-type and V60 and F62 mutants of IFABP monitored by circular dichroism

The equilibrium unfolding transition of IFABP and its fluorescently labeled mutants was monitored by far UV circular dichroism (CD) measurements at 216 nm, and the data were fit to a two-state model (Santoro and Bolen, 1988, 1992). The thermodynamic parameters obtained from the fit for wild-type IFABP and for the corresponding labeled proteins (V60Flu, V60Alexa, F62Flu, and F62Alexa) are given in Table 1. It should be noted that although the Alexa-modified proteins are somewhat less stable compared to that of the wild-type IFABP, their equilibrium unfolding properties match reasonably well with those of the

TABLE 1 Parameters obtained from the Gdn-induced unfolding of different IFABP mutants

Mutants	ΔG^{0}* kcal mol^{-1}	$m^{\dagger}$ kcal mol^{-1}M^{-1}	midpoint (M)
V60Alexa	4.9	−4.3	1.1
V60Flu	3.4	−3.3	1.0
F62Alexa	2.3	−2.7	0.9
F62Flu	3.4	−3.7	0.9

*ΔG^{0}, free energy of unfolding extrapolated to zero Gdn concentration.
†m, slope of the dependence of free energy of unfolding (ΔG) with Gdn concentration.

fluorescein analogs. However, the unfolding transition for F62Alexa is less cooperative than the other proteins. It was shown earlier that the insertion of the fluorescein probes at different positions of IFABP did not perturb the structure or the folding characteristics of the protein to any significant extent (Frieden et al., 1995).

Correlation functions observed for F62Alexa in the presence of different concentrations of Gdn

Plots of the correlation function observed for F62Alexa at different Gdn concentrations are shown in Fig. 2. At every denaturant concentration, the correlation data are best fit with a model containing a diffusion component (τ_D) (Eq. 1), and the residual distributions of the fit at different concentrations are shown in Fig. 2. The diffusion coefficient of the protein in its native state (in the absence of Gdn) calculated as 1.41×10^{-6} cm^2/s using Eq. 3 (as W for our system is known from rhodamine 6G experiments, see above), which matches with the diffusion coefficient expected for a protein with the size of IFABP (15 kDa). However, the variation of τ_D with Gdn concentration did not follow the unfolding transition of the protein monitored by a traditional technique like CD or steady-state fluorescence (data not shown). Moreover, both an abnormal increase in the number of particles and a large decrease in total fluorescence counts were observed with the increase in the denaturant concentrations. The increase in the number of particles with Gdn concentration could not be explained by aggregate formation as that would decrease, rather than increase, the number of particles.

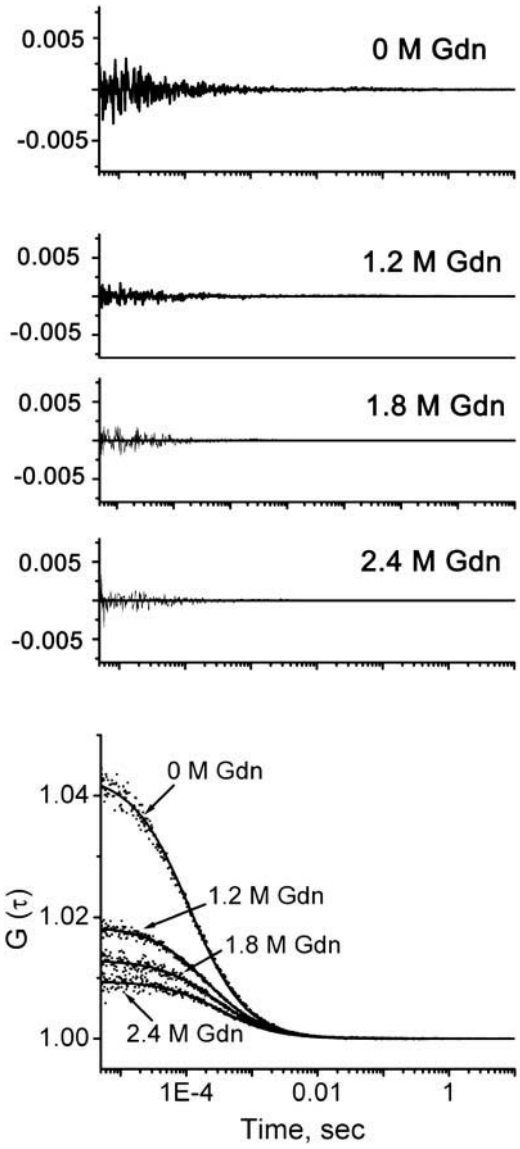

FIGURE 2 Correlation functions of F62Alexa as a function of Gdn concentration. The Gdn concentrations are shown. The lines through the points are obtained from the fit of the correlation function data using Eq. 1, and the residual distributions at each Gdn concentration are shown in the bottom panel. From the amplitude of the curve, it would appear that the number of fluorescent molecules in the beam increases with increasing Gdn (see text). The experiments were performed at room temperature using 20 mM phosphate buffer, pH 7.3. Solutions of F62Alexa at different Gdn concentrations were equilibrated for 1 h before FCS experiments were performed.

Effects of viscosity and refractive index

An increase in Gdn concentration leads to a significant change in the viscosity as well as the refractive index of the solution. The diffusion coefficient (D) is inversely proportional to the viscosity of the medium (consequently τ_D is directly proportional to the viscosity) and hence it would be expected that the diffusion time would change linearly with an increase in Gdn concentration. On the other hand, the increase in the Gdn concentration increases the refractive index of the medium, which leads to refractive index mismatch between the immersion medium of the objective (water) and the sample solution.

Refractive index mismatch

The refractive index mismatch and related aberration in microscopy have been discussed in great detail (Booth et al., 2002; Booth and Wilson, 2000, 2001; Bucher et al., 2000;

Hell et al., 1993; Watson, 1997), and Fig. 3 shows a standard geometrical representation of the aberration. If the refractive indices of both the media are the same ($n_1 = n_2$), there is no aberration. Often n_1 is not equal to n_2, resulting in aberration. Visser et al. (1992) have shown that

$$d_N = \frac{\tan[\sin^{-1}(NA/n_1)]}{\tan[\sin^{-1}(NA/n_2)]} d_A, \quad (4)$$

where d_N is the distance between the focal position in the nonaberrated condition and the interface (Fig. 3); d_A is the actual distance in presence of aberration (Fig. 3) and NA is the numerical aperture of the objective.

The effects of aberration and the subsequent loss of axial resolution have been studied by Sheppard (2000) and Wilson and Carlini (1989). They used a vectorial and a scalar theory, respectively. Hell et al.(1993) have calculated the point spread function in an optically mismatched medium and predicted quantitatively the decrease in resolution, intensity drop, and the focus shift. Their results suggest that for an oil immersion objective with a numerical aperture of 1.3 and at 514 nm, the peak intensity is 40% less for a fluorescent plane 20 μm deep inside an aqueous medium compared to when it is 10 μm deep.

Correction strategies for the refractive index mismatch

Different groups have studied the effects of aberrations in microscopy and several methods have also been proposed to compensate for this effect (Booth and Wilson, 2001; Sheppard, 2000; Sherman et al., 2002). Booth and coworkers have recently discussed strategies of correcting for specimen-induced spherical aberration in confocal microscopy of skin. They include using an iris to reduce the pupil area of an objective, changing the refractive index of the immersion medium to match the specimen refractive index, and using a lens with variable coverglass correction (Booth and Wilson, 2000). Fig. 2 shows the correlation function observed for F62Alexa in the absence and in the presence of different concentrations of Gdn (that is, in the presence of aberrations). The correlation function data of F62Alexa still fits Eq. 1 (which contains a single diffusion component) at every Gdn concentration as indicated by the randomness of the residual distribution. No second component is needed. The same result has been observed in the experiments with the free dye, Alexa488 maleimide (data not shown). This suggests that, although the refractive index mismatch leads to a poorly defined observation volume, the experimental correlation function still fits to a three-dimensional Gaussian beam shape in the concentration range of the Gdn concentrations we have studied. It has been noted that the deviation from the Gaussian approximation can lead to an additional artifactual component in the correlation function, although this effect is mostly prominent for one photon excitation when a large pinhole aperture is used (Hess and Webb, 2002).

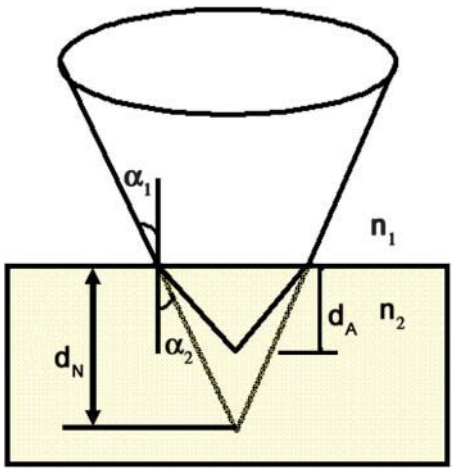

FIGURE 3 Geometrical representation of the refractive index mismatch between two media with refractive indices of n_1 and n_2 ($n_2 > n_1$).

To determine the effects of refractive index mismatch, we have carried out a series of experiments on Alexa488 maleimide in the presence of different concentrations of Gdn. The correction collar of the objective and the height between the objective and the coverslip have been systematically changed to obtain the optimum conditions for the FCS measurements at each Gdn concentration. Alexa488 maleimide has been chosen for these experiments instead of the protein because Gdn solutions should have no effect on the structure and conformation of the free dye.

In the first set of experiments, the objective was placed in such a way that the focal point remains deep inside the solution, which guarantees significant aberration in a mismatched condition. At each Gdn concentration, the objective correction collar was systematically changed and the correlation functions have been fitted to Eq. 1. Fig. 4 *a* shows the correlation functions observed for Alexa488 maleimide in presence of 0 M and 2 M Gdn with various collar settings. When the collar setting is 0.13, a large decrease in the amplitude of the correlation function ($G(0)$) is evident in the presence of 2 M Gdn. A small increase of $G(0)$ takes place when the collar setting is changed to 0.17. With a collar setting of 0.21, an almost complete recovery of $G(0)$ results (Fig. 4 *a*). Fig. 4 *b* plots the variation of counts with different collar settings in the presence of different concentrations of Gdn. It is evident that although the intensity (or counts) goes up significantly with the collar setting in the presence of 2 M Gdn, the trend is reversed for the dye in the absence of Gdn. However, in the presence of an intermediate concentration of Gdn, e.g., 0.9 M Gdn, the count increases to a maximum at a collar setting of 0.15 and decreases thereafter (Fig. 4 *b*). Thus, Fig. 4 *b* suggests that the change in collar setting does compensate for the aberration in presence of 2 M Gdn. In presence of 0.9 M Gdn, it corrects

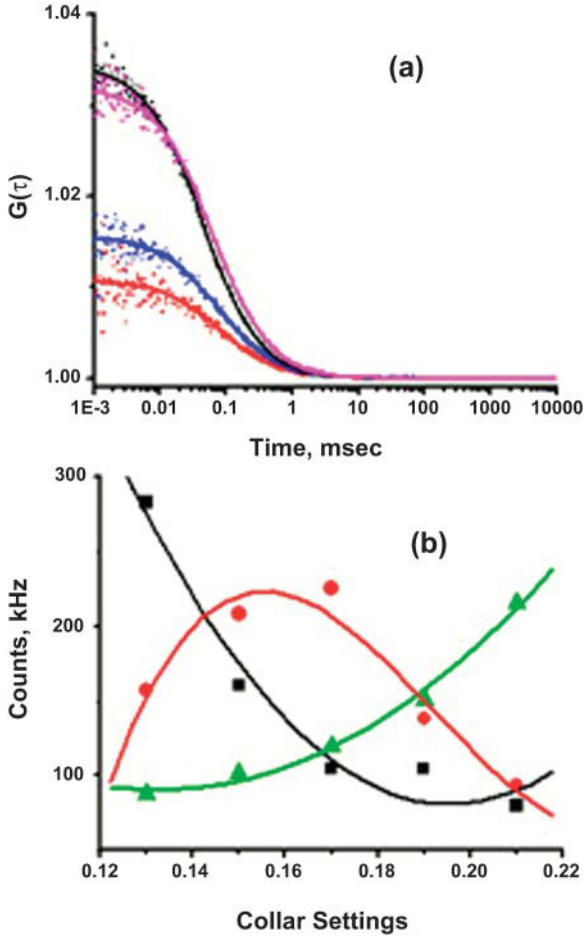

FIGURE 4 (*a*) Correlation functions observed for Alexa488 maleimide in the presence of 0 M Gdn with the collar setting of 0.13 (*black*), 2 M Gdn with the collar setting of 0.13 (strongly aberrated condition, *red*), 2 M Gdn with the collar setting of 0.17 (*blue*) and, 2 M Gdn with the collar setting of 0.21 (*magenta*). (*b*) Variation of the counts with different collar settings in the presence of 0 M (*black*), 0.9 M (*red*), and 2 M Gdn (*green*). Experiments were done with the free dye, Alexa488 maleimide, at room temperature in the presence of 20 mM potassium phosphate buffer, pH 7.3. The lines drawn through the points in *b* are fit using a polynomial function to show the trend.

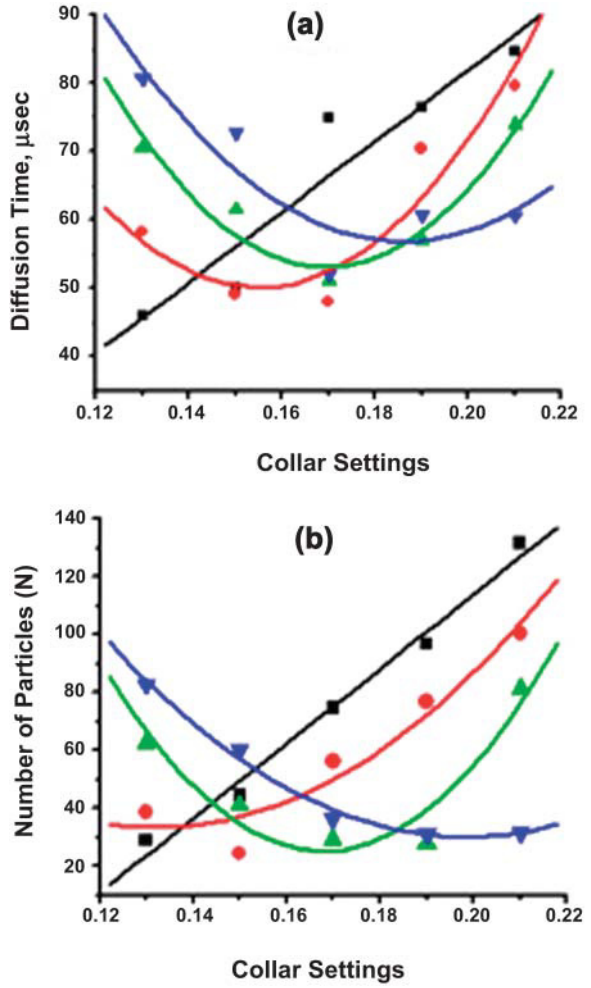

FIGURE 5 Dependence of the (*a*) diffusion time and (*b*) the number of particles of Alexa488 maleimide with the correction collar in the presence of 0 M (*black*), 0.6 M (*red*), 1.2 M (*green*), and 1.8 M Gdn (*blue*). The experimental conditions were described in Fig. 4.

initially and after 0.17, it overcorrects the aberration. In the absence of Gdn, it starts overcorrecting at the lowest collar setting.

Fig. 5, *a* and *b*, show variation of τ_D and N with changes in the correction collar at four different Gdn concentrations, namely, 0 M, 0.6 M, 1.2 M, and 1.8 M Gdn. In all Gdn concentrations except 0 M, an aberration has been introduced as a result of refractive index mismatch. Increasing the collar settings compensates for the mismatch initially, and beyond an optimal collar setting, overcompensates. Consequently, variation of τ_D and N with collar setting reaches a minimum at each Gdn concentration except 0 M Gdn (Fig. 5, *a* and *b*). In the case of 0 M Gdn, there is no refractive index mismatch and hence the increase in collar setting overcorrects from the beginning, leading to a linear increase in both the parameters.

In the second set of experiments, the collar has been set to a value where τ_D and N are at their minima at each Gdn concentration (Fig. 5). The position of the objective was then changed systematically, and correlation functions have been obtained at each position. Fig. 6, *a* and *b*, show, in the presence of 0 M, 0.6 M, 1.2 M, and 1.8 M Gdn and at two different collar settings, the dependence of τ_D and N with the height, i.e., the distance between the focal point and the surface of the coverslip. At 0 M Gdn with the collar setting of 0.13, there is no aberration, and no height dependence was observed for these parameters. In the presence of 0.6 M Gdn, τ_D and N decrease initially with the height and then increase, and at an intermediate range, no change occurs. For 1.2 M and 1.8 M Gdn, τ_D and N decrease linearly and then plateau. It would have been interesting to see at these two Gdn concentrations whether τ_D and N begin to increase (as with 0.6 M Gdn) with further increase in height. That experiment, however, was not possible because increasing the

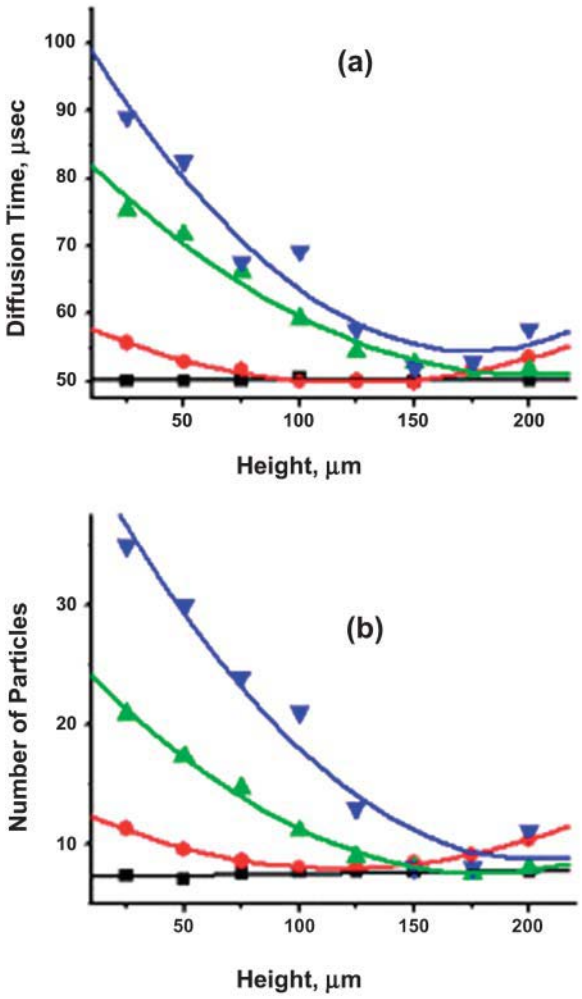

FIGURE 6 Dependence of the (*a*) diffusion time and (*b*) the number of particles of Alexa488 maleimide with the height between the objective and the coverslip surface in the presence of 0 M (*black*), 0.6 M (*red*), 1.2 M (*green*), and 1.8 M Gdn (*blue*).

height of the objective would cause it to touch the coverslip surface.

Unfolding transitions of F62Alexa and V60Alexa monitored by FCS after viscosity and refractive index correction

The above experiments on Alexa488 maleimide allow us to determine an optimum collar setting and a range of distances between the focal point and the coverslip surface at which τ_D and N reach a minimum and the refractive index mismatch is minimal or absent. FCS experiments on F62Alexa were carried out at these optimum conditions so that the data obtained on protein samples should not have any refractive index artifact. The diffusion time (τ_D) data obtained from F62Alexa at each position was further calibrated with the dye diffusion time at that point so that the viscosity effect could also be normalized. Fig. 7 shows that the Gdn dependence of the τ_D values of F62Alexa corrected for the viscosity effect and refractive index mismatch agrees well with the unfolding transition of the same protein monitored by CD. The inset of Fig. 7 shows the change in number of particles of F62Alexa with Gdn. In contrast to the aberrated condition, no systematic change in the number of particle was observed.

To check further the validity of this method, we used this method with a second IFABP mutant, V60Alexa. As before, the τ_D values in the presence of refractive index mismatch did not show any physically meaningful variation with Gdn concentration and no unfolding transition was observed (data not shown). A variation of the number of particles was also observed with Gdn concentration. However, after the mismatch has been corrected by the method described above, the unfolding transition of V60Alexa monitored by the FCS measurements closely matched with that monitored by far UV CD (data not shown).

Variation of τ_R with Gdn concentrations

As we have shown previously (Chattopadhyay et al., 2002a), the correlation function observed for V60Flu could not be fit to a simple diffusion model (Eq. 1), and a model containing a diffusion component (with the diffusion time of τ_D) and an exponential component (τ_R) (Eq. 2) had to be used. The exponential component was interpreted as the time constant of an isomerization reaction in the native state of V60Flu, involving quenching of the fluorescein dye by Trp-82. For the Alexa modified protein (V60Alexa), however, the quenching of Alexa fluorescence by Trp-82 is less and, consequently, the amplitude of the isomerization signal is smaller. We have studied V60Flu to measure the dependence of both the correlation time (τ_R) and the amplitude of the isomerization (A) as a function of Gdn concentration. Fig. 8 shows that the amplitude of the V60Flu isomerization

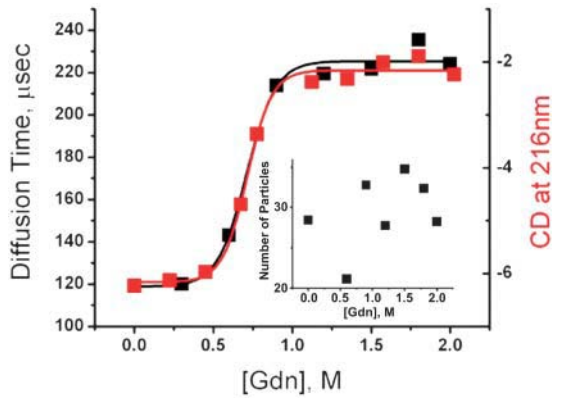

FIGURE 7 Unfolding transitions of F62Alexa monitored by CD (*red*) and corrected diffusion time (*black*). The data have been fit successfully using a typical two-state model and the line drawn through the data shows the fit. The inset shows the variation of the corrected number of particles with the concentration of Gdn.

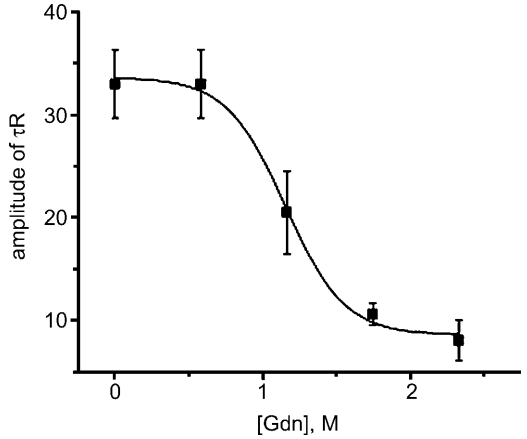

FIGURE 8 Dependence of the amplitude of the relaxation time, τ_R, of V60Flu on the Gdn concentration. The amplitude of τ_R was determined by fitting the correlation function data at different Gdn concentrations using Eq. 2. The experimental conditions were the same as that described in Fig. 3.

decreases significantly with Gdn concentrations, reaching a minimum in the unfolded state of the protein. Although this rate becomes difficult to measure as the amplitude of the isomerization phase decreases, it might be expected to remain relatively unchanged since at any point in the denaturation curve, the protein solution is primarily a mixture of the folded and unfolded forms. The folded form would have a value of τ_R similar to that observed in the absence of denaturant whereas the isomerization step in the unfolded protein would essentially disappear. We would therefore expect that the amplitude, but not the value of τ_R, would mimic the denaturation curve of the protein. A fit of the amplitude of the τ_R process with Gdn concentration leads to a midpoint of 1.15 M similar to that observed in CD experiments (1.01 M, Table 1).

Radius of IFABP at different unfolding conditions

The diffusion coefficients (D) of the protein samples can be obtained directly by FCS experiments using Eq. 3. The apparent hydrodynamic radii (R_H) of the protein in the native state and in the unfolded state can be obtained from the diffusion coefficient using the Stoke-Einstein formulation (Eq. 5) as

$$D = \frac{kT}{6\pi\eta R_H}. \quad (5)$$

Assuming a spherical molecule, the hydrodynamic radii of IFABP under different experimental conditions have been determined and shown in Table 2. The hydrodynamic radius of IFABP in the native state in the absence of any denaturant (16.5 Å) agrees well with the radius (16.4 Å) calculated from the crystal structure volume of IFABP (18479 Å^3). In our previous study, we showed that there was an increase in the hydrodynamic radius of IFABP observed in the acid unfolded form at pH 2 (22 Å). This study shows a further increase in the hydrodynamic radius of IFABP in the presence of 2 M Gdn (31 Å, Table 2). We have performed light-scattering experiments on the V60C mutant of IFABP (unlabeled mutant) to determine the hydrodynamic radii of the protein in the presence of 2 M Gdn. The radius obtained by light-scattering data at this condition (25 Å) matches well with our FCS data.

TABLE 2 Diffusion coefficient and the hydrodynamic radius (R_H) of IFABP determined from the diffusion time measurements under different unfolding conditions

	D*, cm^2/s	R_H, Å
V60Alexa in the native state	1.4×10^{-6}	17
V60Alexa unfolded (in presence of Gdn)	0.8×10^{-6}	31
V60Alexa unfolded (at pH 2)†	1.1×10^{-6}	22
F62Alexa unfolded (in presence of Gdn)	0.7×10^{-6}	31
V60C unfolded (in presence of Gdn)‡		25

Experiments were performed at room temperature using 20 mM phosphate buffer, pH 7.3.
*Diffusion coefficient calculated from the τ_D values. Errors are within ±10%.
†Taken from Chattopadhyay et al. (2002a).
‡Data obtained from light-scattering experiments.

DISCUSSION

Fluorescence correlation spectroscopy: advantages and artifacts

FCS has been used to monitor changes in the diffusion coefficient in biological systems. It also has great potential to be used as a tool to investigate conformational dynamics in complex biological systems (Elson, 1985; Hess et al., 2002). An important parameter that can be obtained from FCS is the number of particles in the observation volume, which is a very sensitive measure of the presence of aggregation or of a monomer-dimer equilibrium in solution. The advantages of FCS are that it can be used at a very low concentration (typically 10–50 nM); it is an equilibrium technique and hence no external perturbation is needed and it has high sensitivity and wide timescales.

There are, however, a number of artifacts that can influence results from FCS measurements. Hess and Webb have shown that the conventional assumption of a three-dimensional Gaussian observation volume does not hold well for confocal optics at large detector aperture (Hess and Webb, 2002) leading to erroneous diffusion time values as well as observation of spurious diffusion components. The reason for the non-Gaussian observation volume is the diffraction of light by the aperture. There are two ways of overcoming that problem. The first is to use a small detector aperture or underfilled back aperture, even though that reduces the signal/noise ratio. The second is to use two-photon excitation, as used here, which leads to a nearly Gaussian observation volume. We have observed that the mismatch in the refractive

index between the sample and the immersion medium leads to an increase in the diffusion time as well as affecting significantly the apparent number of particles.

Correcting refractive index mismatch

We have shown that careful and detailed experiments are necessary to minimize aberrations in FCS measurements performed on solutions with different indices of refraction. Using a fluorophore, the diffusion coefficient of which is not affected by changes in solution conditions, we changed the correction collar and the position of the objective systematically to achieve the optimum condition for the FCS experiments. The following paragraphs will describe some of the features of the optimum condition at which the refractive index mismatch is minimal or absent.

First, the refractive index mismatch and consequent aberration leads to a significant decrease in the total photon counts. Hence a large increase in the counts and consequently a much improved signal/noise ratio can be achieved at this optimum condition. This decreases the average data acquisition time quite significantly.

Second, the τ_D and N have been found to be at their minimum in aberration-compensated condition. Since $G(0)$, the amplitude of the correlation function, is inversely proportional to N, in the absence of refractive index aberration, the observation volume is at minimum and hence $G(0)$ is at its maximum. This is particularly important in the case of rapid dynamics measurements for which increasing $G(0)$ significantly enhances the sensitivity of the rate and amplitude determination. Furthermore, the observation volume is increased artificially in an aberrated condition, increasing both τ_D and N, which might create further problems in dynamics measurements. It has been observed before that nonideality in the observation profile results in the appearance of an extra component in the correlation function, which can be mistaken as a kinetics component (Hess and Webb, 2002). Moreover, an artificial increase in the number of particles as a result of refractive index mismatch can as well be incorrectly inferred as disaggregation in solution studies or differential localization of a fluorophore in a typical FCS experiment inside a cell sample. Also, an aberrated increase in τ_D can result in errors both in diffusion coefficient and in laser beam radius measurements. In FCS experiments in cells, localized differences in refractive index could cause changes in the apparent observation profile, leading to artifactual changes in particle number.

Third, although in our experiments with Alexa488 maleimide we have seen that the correlation functions observed in a mismatched condition can be fit to an ellipsoidal Gaussian intensity profile, yielding a random residual distribution in diffusion measurements, the height/waist ratio (S) does not converge. S is an important parameter to define the observation volume in the three-dimensional Gaussian approximation, and it has been shown before that non-Gaussian behavior of the observation volume leads to an artificial increase in this parameter that often diverges when the observation volume is strongly non-Gaussian. When the refractive index mismatch has been minimized by selecting optimum collar and objective position, S converges to a physically meaningful number. Fig. 9 shows the values of S determined at each Gdn concentration under conditions at which the refractive index mismatch is minimized by our method. The number at 0 M Gdn represents S when there is no mismatch. This is obtained in a calibration experiment to determine the quality of the alignment and laser conditions in our setup. The agreement between S values observed in Gdn samples and that at 0 M Gdn reflects that this method corrects the mismatch well.

The native state, the unfolded states, and the folding of IFABP

The unfolding transition monitored by the change in diffusion time (refractive index and viscosity corrected) for all the IFABP mutants matches well with that observed by CD and steady-state tryptophan fluorescence, indicating that the unfolding of secondary structure, tertiary structure, and increase in the overall size of the protein occur simultaneously without substantial accumulation of intermediate states in equilibrium. It has been shown before that coupling of a dye like fluorescein at different positions of IFABP does not have any adverse effect on the folding of this protein (Frieden et al., 1995).

The folding kinetics of IFABP has been studied in great detail, and two kinetic intermediates have been demonstrated by a combination of stopped flow and continuous flow experiments (Chattopadhyay et al., 2002b). However, the

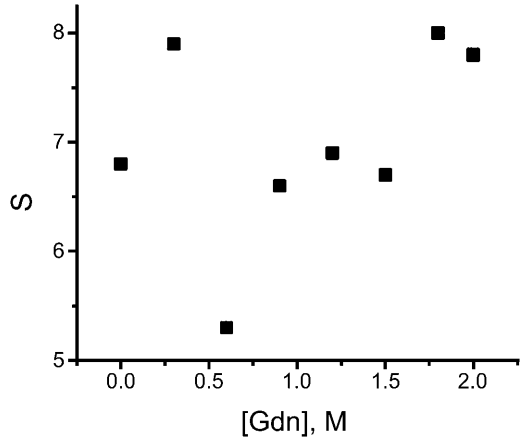

FIGURE 9 Variation of the height/width ratio (S) observed with Alexa488 maleimide in the aberration compensated condition with Gdn concentration. The experimental condition is as described in Fig. 4. The value of S has been converged at each condition and is similar to that observed in the absence of Gdn.

formation of the first intermediate could not be followed as it occurs extremely rapidly, faster than the dead time of the continuous flow mixer we had used previously (~100 μs). FCS experiments indicate a significant contribution of a fast process with a correlation time of 35 μs, which disappears upon unfolding of the protein at pH 2 and also in the presence of 2 M Gdn. Although it is tempting to link this motion with the fast unresolved folding kinetics of IFABP, we could not obtain any direct experimental evidence to support this. However, it should be noted that if τ_R is strongly coupled to the unfolding kinetics, we would expect its amplitude to be at a maximum and its value to be at a minimum at the middle of the transition. This is definitely not the case, suggesting that τ_R may not be coupled strongly to the major unfolding kinetics.

The unfolded state of a protein is of prime interest. Although it has been envisioned as a random coil, recent findings suggest that the presence of structural elements in the unfolded state are important for efficient folding (Creamer et al., 1995; Dill and Shortle, 1991; Pappu and Rose, 2002). To understand the mechanism of protein folding, it is essential to characterize the unfolded state, and it is also important to understand how different unfolding agents, such as acid, Gdn, or urea affect the unfolded state of a protein. Millett et al. (2002) have recently reviewed a large number of small-angle x-ray and neutron scattering studies and listed the radii of native and unfolded states of different proteins. They note that the unfolded states obtained by different chemically denaturing agents like urea or Gdn are identical and are highly expanded, coil-like configurations. Millett et al. (2002), using Eq. 6 define, the relationship between polymer length and the radius of gyration under different solvent conditions as

$$R = R_0 N^{\upsilon}, \tag{6}$$

where N is the number of monomers in the polymer chain or the number of residues in the protein, R_0 is a constant, and υ is an exponential scaling factor. R_0 is a function of the persistence length and υ is a function of the nature of solvent. Fig. 10 shows a plot of radii of gyration of different proteins determined by x-ray and neutron scattering in a highly denaturing condition as function of the number of residues, taken from the study of Millett et al. (2002). The black solid line is the fit of the data using Eq. 6 with $\upsilon = 0.59$, a value close to what is expected for a random coil (0.588) Since FCS measures the hydrodynamic radius (R_H) and not the radius of gyration (R_G), Fig. 10 also shows a plot of R_H values of different proteins at their native (*red*) and chemically unfolded states (*green*) as a function of persistent length (taken from Wilkins et al., 1999). The hydrodynamic radii (R_H) of IFABP at pH 2 and in the presence of 2 M Gdn are also shown in Fig. 10 for comparison. Although the radius at pH 2 matches well with the R_H of the native proteins, the data in the presence of 2M Gdn falls within the expected range for the random coil structure (Fig. 10).

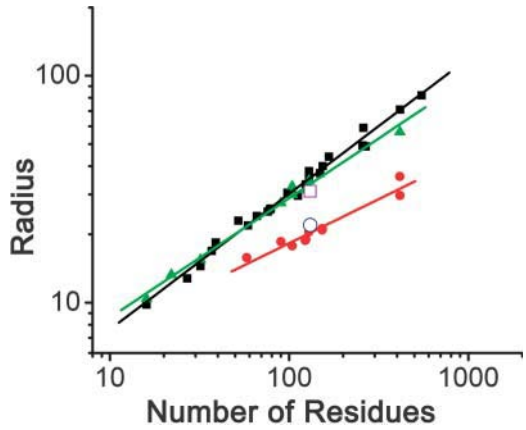

FIGURE 10 Variation of radii of gyration (*black*) and hydrodynamic radii (*green*) of different proteins (lacking disulfide bonds) unfolded by chemical denaturant like urea or Gdn with the number of amino acid residues. Variation of hydrodynamic radii of different proteins at their native state in ''poor'' solvent with the number of amino acid residues is also shown (*red*). The lines are the fit of the data using Eq. 7. The hydrodynamic radii of IFABP (R_H) in the presence of 2 M Gdn (□) and at pH 2 (○) are also shown in the figure as open symbols.

Understanding the unfolded states of a protein remains an elusive goal. Although residual dipolar coupling measurements indicate the persistence of a native-like structure in the unfolded states (Dill and Shortle, 1991; Ohnishi et al., 2004), data from small-angle x-ray and neutron scattering studies indicate the radius of the unfolded state in Gdn or urea (''good solvent'') matches well with the random coil predictions (Kohn et al., 2004). Our FCS data also support that observation. A recent study has consolidated these two apparently conflicting results (Fitzkee and Rose, 2004). They have shown that a random coil-like radius can be generated in a protein by randomizing only 8% of its native contacts and hence suggested that observation of a random coil-like radius in the unfolded state does not necessarily rule out the possibility of transient structural formation. Experiments are currently under way in our laboratory to develop applications of FCS to understand the dynamics of the unfolded states.

CONCLUSION

FCS has been used to study the diffusional and conformational dynamics of IFABP in the presence of different concentrations of Gdn. FCS experiments using V60Flu show the presence of a conformational fluctuation with a relaxation time (τ_R) on the order of 35 μs in the native state of the protein. Due to the effects of viscosity and the refractive index of Gdn solutions, the FCS observation volume changes, leading to an apparent increase in the diffusion time (τ_D) and the number of particles (N). We have studied this aberration in detail and corrected our data utilizing the objective correction collar to minimize and correct the refractive index and viscosity effects. The amplitude of

the conformational dynamics (τ_R) decreases sharply as the protein unfolds with pH or in the presence of Gdn. Although the unfolded state of IFABP at pH 2 is compact and native-like, the radius of the protein in presence of 2 M Gdn falls within the range expected for a random coil.

This work was supported by National Institutes of Health grants DK13332 (C.F.) and GM38838 (E.L.E.).

REFERENCES

Booth, M. J., M. A. Neil, M. R. Juskaitis, and T. Wilson. 2002. Adaptive aberration correction in a confocal microscope. *Proc. Natl. Acad. Sci. USA.* 99:5788–5792.

Booth, M. J., and T. Wilson. 2000. Strategies for the compensation of specimen-induced spherical aberration in confocal microscopy of skin. *J. Microsc.* 200:68–74.

Booth, M. J., and T. Wilson. 2001. Refractive-index-mismatch induced aberrations in single-photon and two-photon microscopy and the use of aberration correction. *J. Biomed. Opt.* 6:266–272.

Bucher, D., M. Scholz, M. Stetter, K. Obermayer, and H. J. Pfluger. 2000. Correction methods for three-dimensional reconstructions from confocal images: I. Tissue shrinking and axial scaling. *J. Neurosci. Methods.* 100:135–143.

Chattopadhyay, K., S. Saffarian, E. L. Elson, and C. Frieden. 2002a. Measurement of microsecond dynamic motion in the intestinal fatty acid binding protein by using fluorescence correlation spectroscopy. *Proc. Natl. Acad. Sci. USA.* 99:14171–14176.

Chattopadhyay, K., S. Zhong, S.-R. Yeh, D. L. Rousseau, and C. Frieden. 2002b. The intestinal fatty acid binding protein: the role of turns in fast and slow folding processes. *Biochemistry.* 41:4040–4047.

Creamer, T. P., R. Srinivasan, and G. D. Rose. 1995. Modeling unfolded states of peptides and proteins. *Biochemistry.* 34:16245–16250.

Dill, K. A., and D. Shortle. 1991. Denatured states of proteins. *Annu. Rev. Biochem.* 60:795–825.

Elson, E. L. 1985. Fluorescence correlation spectroscopy and photobleaching recovery. *Annu. Rev. Phys. Chem.* 36:379–406.

Fitzkee, N. C., and G. D. Rose. 2004. Reassessing random-coil statistics in unfolded protein. *Proc. Natl. Acad. Sci. USA.* 101:12497–12507.

Frieden, C., K. Chattopadhyay, and E. L. Elson. 2002. What fluorescence correlation spectroscopy can tell us about unfolded proteins. *Adv. Protein Chem.* 62:91–110.

Frieden, C., N. Jiang, and D. P. Cistola. 1995. Intestinal fatty acid binding protein: folding of fluorescein-modified proteins. *Biochemistry.* 34:2724–2730.

Haupts, U., S. Maiti, P. Schwille, and W. W. Webb. 1998. Dynamics of fluorescence fluctuations in green fluorescent protein observed by fluorescence correlation spectroscopy. *Proc. Natl. Acad. Sci. USA.* 95: 13573–13578.

Hell, S. W., G. Reiner, C. Cremer, and E. H. K. Stelzer. 1993. Aberrations in confocal microscopy induced by mismatches in refractive index. *J. Microsc.* 169:391–405.

Hess, S. T., and W. W. Webb. 2002. Focal volume optics and experimental artifacts in confocal fluorescence correlation spectroscopy. *Biophys. J.* 83:2300–2317.

Hess, S. T., S. Huang, A. A. Heikal, and W. W. Webb. 2001. Biological and chemical applications of fluorescence correlation spectroscopy: a review. *Traffic.* 2:789–796.

Hess, S. T., S. Huang, A. A. Heikal, and W. W. Webb. 2002. Biological and chemical applications of fluorescence correlation spectroscopy: a review. *Biochemistry.* 41:697–705.

Hodsdon, M. E., J. W. Ponder, and D. P. Cistola. 1996. The NMR solution structure of intestinal fatty acid-binding protein complexed with palmitate: application of a novel distance geometry algorithm. *J. Mol. Biol.* 264:585–602.

Jiang, N., and C. Frieden. 1993. Intestinal fatty acid binding protein: characterization of mutant proteins containing inserted cysteine residues. *Biochemistry.* 32:11015–11021.

Kohn, J. E., I. S. Millett, J. Jacob, B. Zagrovic, T. M. Dillon, N. Cingel, R. S. Dothager, S. Seifert, P. Thiyagarajan, T. R. Sosnick, M. Z. Hasan, V. S. Pande, I. Ruczinski, S. Doniach, and K. W. Plaxco. 2004. Random-coil behavior and the dimensions of chemically unfolded proteins. *Proc. Natl. Acad. Sci. USA.* 101:12491–12496.

Millett, I. S., S. Doniach, and K. W. Plaxco. 2002. Toward a taxonomy of the denatured state: small angle scattering studies of unfolded proteins. *Adv. Prot. Chem.* 62:241–262.

Ohnishi, S., A. L. Lee, M. H. Edgell, and D. Shortle. 2004. Direct demonstration of structural similarity between native and denatured eglin C. *Biochemistry.* 43:4064–4070.

Pappu, R. V., and G. D. Rose. 2002. A simple model for polyproline II structure in unfolded states of alanine-based peptides. *Protein Sci.* 11: 2437–2455.

Sacchettini, J. C., J. I. Gordon, and L. J. Banaszak. 1989. Refined apoprotein structure of rat intestinal fatty acid binding protein produced in *Escherichia coli*. *Proc. Natl. Acad. Sci. USA.* 86:7736–7740.

Santoro, M. M., and D. W. Bolen. 1988. Unfolding free energy changes determined by the linear extrapolation method. 1. Unfolding of phenylmethanesulfonyl alpha-chymotrypsin using different denaturants. *Biochemistry.* 27:8063–8068.

Santoro, M. M., and D. W. Bolen. 1992. A test of the linear extrapolation of unfolding free energy changes over an extended denaturant concentration range. *Biochemistry.* 31:4901–4907.

Sheppard, C. J. 2000. Analysis of spherical aberration of a water immersion objective: application to specimens with refractive index 1.33–1.40. *J. Microsc.* 200:177–178.

Sherman, L., J. Y. Ye, O. Albert, and T. B. Norris. 2002. Adaptive correction of depth-induced aberrations in multiphoton scanning microscopy using a deformable mirror. *J. Microsc.* 206:65–71.

Visser, T. D., J. L. Oud, and G. J. Brakenhoff. 1992. Refractive index and axial distance measurements in 3-D microscopy. *Optik.* 90:17–19.

Watson, T. F. 1997. Fact and artefact in confocal microscopy. *Adv. Dent. Res.* 11:433–441.

Wilkins, D. K., S. B. Grimshaw, V. Receveur, C. M. Dobson, J. A. Jones, and L. J. Smith. 1999. Hydrodynamic radii of native and denatured proteins measured by pulse field gradient NMR techniques. *Biochemistry.* 38:16424–16431.

Wilson, T., and A. R. Carlini. 1989. The effect of aberrations on the axial response of confocal imaging systems. *J. Microsc.* 154:243–256.